VII International Conference on Computational Methods for Coupled Problems in Science and Engineering
COUPLED PROBLEMS 2017
M. Papadrakakis, E. Oñate and B. Schrefler (Eds)

NUMERICAL SIMULATION OF TUBE-BUNDLE FLOW-INDUCED VIBRATIONS BY USING THE LS-STAG IMMERSED BOUNDARY METHOD

VALERIA V. PUZIKOVA* AND ILIA K. MARCHEVSKY†

*Applied Mathematics dep., Bauman Moscow State Technical University
105005 Moscow, Russia, 2nd Baumanskaya, 5
e-mail: vvp@dms-at.ru

†Applied Mathematics dep., Bauman Moscow State Technical University
105005 Moscow, Russia, 2nd Baumanskaya, 5
e-mail: iliamarchevsky@mail.ru

Key words: Immersed Boundary Method, The LS-STAG Method, Flow-Induced Vibrations, Bundles of Tubes, Airfoil

Abstract. The LS-STAG method is used in the present study for simulation of tube-bundle flow-induced vibrations. Staggered and in-line tube-bundles are considered. Flow regimes at different distances between tubes are investigated. Oscillations amplitudes for tubes from different bundle columns are computed. The LS-STAG method allows to simulate flow-induced vibrations of these tube-bundles on a very coarse mesh.

1 INTRODUCTION

Flow-induced vibrations occur in tubes of heat exchangers and reactor rod systems under the influence of unsteady hydrodynamic forces. These vibrations can cause the destruction of the whole device due to incorrect choice of working flow velocities. Therefore, simulation of tube-bundle flow-induced vibrations is a very important problem.

To simulate these flow-induced vibrations it is necessary to solve coupled hydroelastic problem. Such problems are complicated for numerical solution, since it is necessary to take into account interference between the flow and moving immersed body. In case of sufficiently massive body, coupled hydroelastic problems can be solved using step-by-step numerical algorithm, firstly simulating flow around a body moving with known parameters and then computing the dynamics of the body with known hydrodynamic loads.

Immersed boundary methods [1] are useful for numerical simulation in coupled hydroelastic problems, since they do not require a coincidence of cell edges and boundaries of the computational domain, and allow to solve problems when domain shape is irregular or it

changes in the simulation process due to aeroelastic body motion. The main advantage of these methods is that we don't need mesh reconstruction at each time step.

The LS-STAG cut-cell immersed boundary method [2] for viscous incompressible flows simulation combines the advantages of immersed boundary methods and the level-set method. This method allows to solve problems on the Cartesian grid. In contrast to classical immersed boundary methods, the flow variables are computed in the cut-cells, and not interpolated. Numerical analogues of conservation laws satisfaction in all fluid domain cells is a basis of LS-STAG discretization constructing, which allows to obtain physically realistic numerical solution. For these reasons, the LS-STAG method is used in the present study for simulation of tube-bundle flow-induced vibrations. The immersed boundary is represented with the level-set function [3]. Linear systems resulting from the LS-STAG discretization of the Navier-Stokes or Reynolds-averaged Navier-Stokes equations, are solved using the BiCGStab method [4] with the ILU- and multigrid [5, 6] preconditioning. An original algorithm for the solver cost-coefficient estimation [7] is used for the optimal parameters of the multigrid preconditioner choice.

2 GOVERNING EQUATIONS

The problem is considered for 2D unsteady case when the flow around an airfoil assumed to be viscous and incompressible. The continuity and momentum equations are the following:

$$\nabla \cdot \mathbf{v} = 0, \quad \frac{\partial \mathbf{v}}{\partial t} + (\mathbf{v} \cdot \nabla)\mathbf{v} = -\frac{1}{\rho}\nabla p + \nu \Delta \mathbf{v}. \tag{1}$$

The boundary conditions on external boundaries of computational domain are the following:

$$\mathbf{v}\big|_{\text{inlet}} = \mathbf{v}_\infty, \quad \frac{\partial \mathbf{v}}{\partial \mathbf{n}}\Big|_{\text{outlet}} = 0, \quad \frac{\partial p}{\partial \mathbf{n}}\Big|_{\text{inlet\&outlet}} = 0, \tag{2}$$

and boundary conditions on the camber line of the airfoil are no-slip conditions:

$$\mathbf{v}\big|_{\text{airfoil}} = \mathbf{v}^{\text{ib}}, \quad \frac{\partial p}{\partial \mathbf{n}}\Big|_{\text{airfoil}} = 0. \tag{3}$$

Here $\mathbf{v}^{\text{ib}}$ is the velocity of the immersed boundary. The airfoil assumed to be rigid and it can oscillate with 1, 2 or 3 degrees of freedom. Its motion is described by dynamics equations which in the most common form can be written down as the following:

$$\ddot{\mathbf{q}} = \mathbf{\Phi}(\mathbf{q}, \dot{\mathbf{q}}) + \mathbf{Q}^{\text{flow}} + \mathbf{Q}^{\text{ext}}. \tag{4}$$

Here $\mathbf{q}$ is the airfoil generalized coordinates vector, $\mathbf{\Phi}(\mathbf{q}, \dot{\mathbf{q}})$ is determined by elastic and viscous constraints imposed on the airfoil, $\mathbf{Q}^{\text{flow}}$ is the generalized aerodynamic force, $\mathbf{Q}^{\text{ext}}$ is external mass forces vector.

3 NUMERICAL METHOD

The Cartesian mesh with cells $\Omega_{i,j} = (x_{i-1}, x_i) \times (y_{j-1}, y_j)$ is introduced in the rectangular computational domain. It is denoted that $\Gamma_{i,j}$ is the face of $\Omega_{i,j}$ and $\mathbf{x}^c_{i,j} = (x^c_i, y^c_j)$ is the center of this cell. Unknown components $u_{i,j}$ and $v_{i,j}$ of velocity vector $\mathbf{v}$ are computed in the middle of fluid parts of the cell faces. These points are the centers of control volumes $\Omega^u_{i,j} = (x^c_i, x^c_{i+1}) \times (y_{j-1}, y_j)$ and $\Omega^v_{i,j} = (x_{i-1}, x_i) \times (y^c_j, y^c_{j+1})$ with faces $\Gamma^u_{i,j}$ and $\Gamma^v_{i,j}$, respectively (fig. 1).

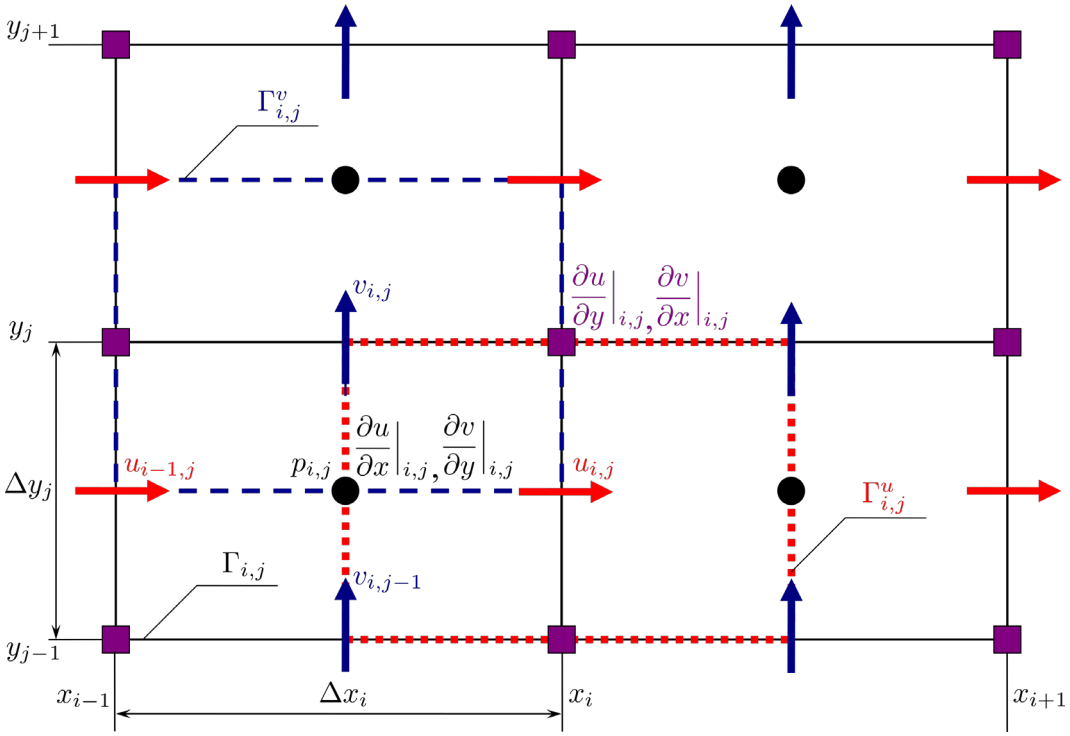

Figure 1: Staggered arrangement of the variables on the LS-STAG mesh

Cells which the immersed boundary intersects are the so-called 'cut-cells' (fig. 2). These cells contain the solid part together with the liquid one. The level-set function φ is used for immersed boundary Γ^{ib} description. The boundary Γ^{ib} is represented by a line segment on the cut-cell $\Omega_{i,j}$. Locations of this segment endpoints are defined by linear interpolation of the variable $\varphi_{i,j} = \varphi(x_i, y_j)$.

The cell-face fraction ratios $\vartheta^u_{i,j}$ and $\vartheta^v_{i,j}$ are introduced. They take values in interval $[0, 1]$ and represent the fluid parts of the east and north faces of $\Gamma_{i,j}$, respectively. One-dimensional linear interpolation of $\varphi(x_i, y)$ on the segment $[y_{j-1}, y_j]$ and $\varphi(x, y_j)$ on the segment $[x_{i-1}, x_i]$ is used for the cell-face fraction ratios computing:

$$\vartheta^u_{i,j} = \frac{\min(\varphi_{i,j-1}, \varphi_{i,j})}{\min(\varphi_{i,j-1}, \varphi_{i,j}) - \max(\varphi_{i,j-1}, \varphi_{i,j})}, \quad \vartheta^v_{i,j} = \frac{\min(\varphi_{i-1,j}, \varphi_{i,j})}{\min(\varphi_{i-1,j}, \varphi_{i,j}) - \max(\varphi_{i-1,j}, \varphi_{i,j})}. \tag{5}$$

According to the concept of the LS-STAG method, normal Reynolds stress components are sampled on the base mesh (similar to pressure discretization) and shear ones are sampled in the upper right corners of the base mesh cells. Thus, for the shear Reynolds stresses an additional mesh (xy-mesh) is introduced. It is denoted that cell $\Omega^{xy}_{i,j} = (x^c_i, x^c_{i+1}) \times (y^c_j, y^c_{j+1})$ is the control volume on the xy-mesh and $\Gamma^{xy}_{i,j}$ represents the faces of this control volume. In case of Reynolds Stress (RSM) RANS models, these meshes are used for transport equation solving for Reynolds stresses. The result then is taken into account in the Helmholtz equation for the velocity. In case of Eddy Viscosity (EVM) RANS models eddy viscosity is sampled on the xy-mesh. It is very suitable that the eddy viscosity at solid boundaries vanishes, so the cut-cells discretization of the eddy viscosity equations and computation of Reynolds stresses becomes simple.

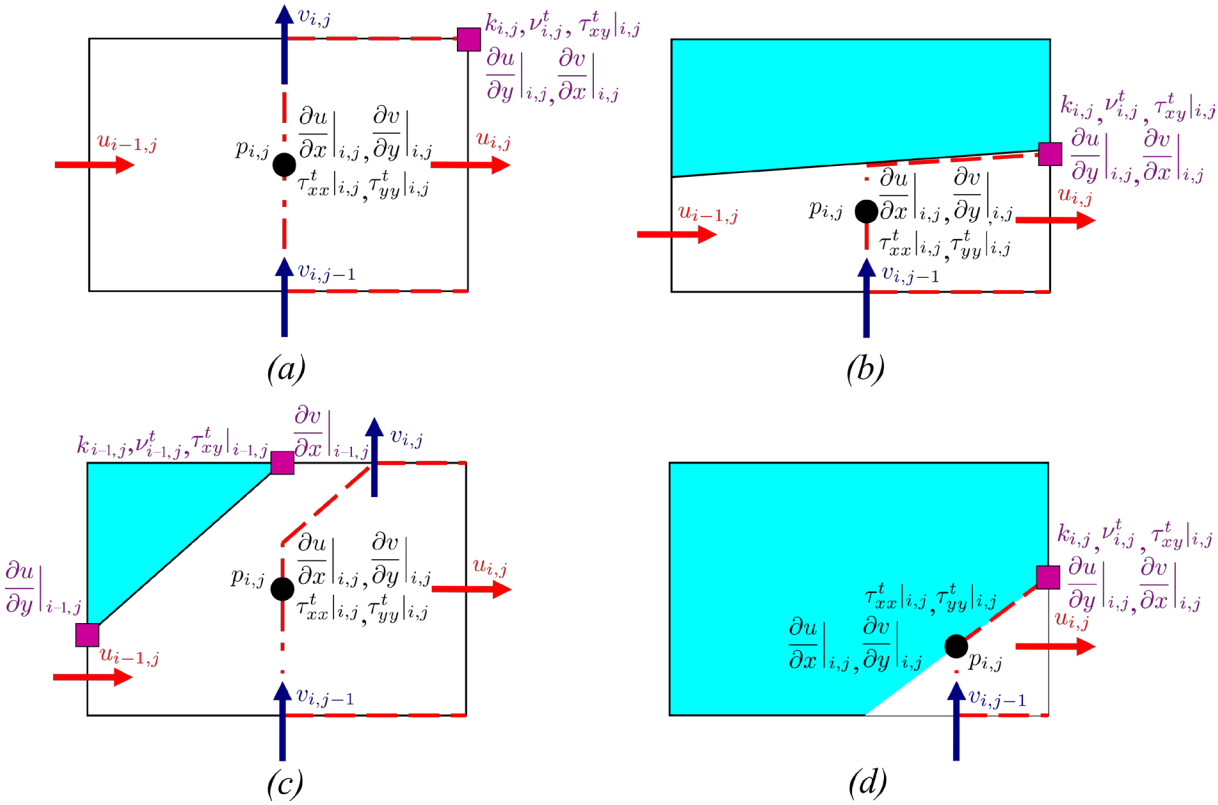

Figure 2: Location of the variables discretization points in the case of generic cells on the LS-STAG mesh: *(a)* Cartesian Fluid Cell; *(b)* North Trapezoidal Cell; *(c)* Northwest Pentagonal Cell; *(d)* Northwest Triangular Cell

Hydrodynamic force can be computed by the following formulae:

$$F_x = \sum_{\text{Cut-cells } \Omega^{ib}_{i,j}} \Big[(\vartheta^u_{i-1,j} - \vartheta^u_{i,j}) \Delta y_j \Big(p_{i,j} - \nu \frac{\partial u}{\partial x}\Big|_{i,j} \Big) - \nu \text{Quad}^{ib}_{i,j} \Big(\frac{\partial u}{\partial y} \mathbf{e}_y \cdot \mathbf{n} \Big) \Big], \tag{6}$$

$$F_y = \sum_{\text{Cut-cells } \Omega^{ib}_{i,j}} \Big[-\nu \text{Quad}^{ib}_{i,j} \Big(\frac{\partial v}{\partial x} \mathbf{e}_x \cdot \mathbf{n} \Big) + (\vartheta^v_{i,j-1} - \vartheta^v_{i,j}) \Delta x_i \Big(p_{i,j} - \nu \frac{\partial v}{\partial y}\Big|_{i,j} \Big) \Big].$$

The quadrature of the shear stresses $\text{Quad}^{ib}_{i,j}$ has to be adapted to each type of cut-cells.

According to the concept of the LS-STAG method, equations (1) should be written in integral form for cell of base mesh, cell of x-mesh and cell of y-mesh respectively:

$$\int\limits_{\Gamma_{i,j}} \mathbf{v} \cdot \mathbf{n} \, dS = 0, \tag{7}$$

$$\frac{d}{dt} \int\limits_{\Omega^u_{i,j}} u \, dV + \int\limits_{\Gamma^u_{i,j}} (\mathbf{v} \cdot \mathbf{n}) u \, dS + \int\limits_{\Gamma^u_{i,j}} p \mathbf{e_x} \cdot \mathbf{n} \, dS - \int\limits_{\Gamma^u_{i,j}} \nu \nabla u \cdot \mathbf{n} \, dS = 0,$$

$$\frac{d}{dt} \int\limits_{\Omega^v_{i,j}} v \, dV + \int\limits_{\Gamma^v_{i,j}} (\mathbf{v} \cdot \mathbf{n}) v \, dS + \int\limits_{\Gamma^v_{i,j}} p \mathbf{e_y} \cdot \mathbf{n} \, dS - \int\limits_{\Gamma^v_{i,j}} \nu \nabla v \cdot \mathbf{n} \, dS = 0.$$

The general form of the LS-STAG discretization for (7) can be written as the following [2]:

$$D^x U_x + D^y U_y + \overline{U}^{ib} = 0, \tag{8}$$

$$\frac{d}{dt}(M^x U_x) + C^x U_x + G^x P - \nu K^x U_x + S^{ib,c}_x - \nu S^{ib,\nu}_x = 0,$$

$$\frac{d}{dt}(M^y U_y) + C^y U_y + G^y P - \nu K^y U_y + S^{ib,c}_y - \nu S^{ib,\nu}_y = 0.$$

Here P is the discrete pressure, U_x and U_y are the discrete components of the velocity vector; $S^{ib,c}_x$, $S^{ib,\nu}_x$, $S^{ib,c}_y$, $S^{ib,\nu}_y$ are source terms; $\overline{U}^{ib}$ is the mass flux; D^x, D^y are the divergence discrete analogues; K^x and K^y represent the discretization of the diffusive terms; C^x and C^y represent the discretization of the convective terms; $G^x = -D^T_x$ and $G^y = -D^T_y$ are the gradient discrete analogues.

The time integration of the differential algebraic system (8) is performed with a semi-implicit Euler scheme. Predictor step leads to discrete analogues of the Helmholtz equation for velocities prediction $\widetilde{U}_x$, $\widetilde{U}_y$ at the time $t_{n+1} = (n+1)\Delta t$:

$$\frac{M^{n+1}_x \widetilde{U}_x - M^n_x U^n_x}{\Delta t} + C^n_x U^n_x + S^{ib,c,n}_x - D^{T,n}_x P^n - \nu K^{n+1}_x \widetilde{U}_x - \nu S^{ib,\nu,n+1}_x = 0, \tag{9}$$

$$\frac{M^{n+1}_y \widetilde{U}_y - M^n_y U^n_y}{\Delta t} + C^n_y U^n_y + S^{ib,c,n}_y - D^{T,n}_y P^n - \nu K^{n+1}_y \widetilde{U}_y - \nu S^{ib,\nu,n+1}_y = 0.$$

Here Δt is a time discretization step. Corrector step leads to the following discrete analogue of Poisson equation for $\Phi = \Delta t(P^{n+1} - P^n)$:

$$A^{n+1}\Phi = D_x^{n+1}\widetilde{U}_x + D_y^{n+1}\widetilde{U}_y + \overline{U}^{ib,n+1}, \tag{10}$$

$A = -D^x(M^x)^{-1}(D^x)^T - D^y(M^y)^{-1}(M^y)^T$. Then flow variables at the time point t_{n+1} are computed by the following formulae:

$$U_x^{n+1} = \widetilde{U}_x + (M_x^{n+1})^{-1}D_x^{T,n+1}\Phi,\ U_y^{n+1} = \widetilde{U}_y + (M_y^{n+1})^{-1}D_y^{T,n+1}\Phi,\ P^{n+1} = \frac{\Phi}{\Delta t} + P^n. \tag{11}$$

4 NUMERICAL EXPERIMENTS

A number of model problems had been considered before simulation of tube-bundle flow-induced vibrations: flow around fixed system of circular airfoils [8], circular airfoil wind resonance and buffeting which are presented below.

4.1 Circular airfoil wind resonance

To simulate wind resonance phenomenon we considered the motion of the circular airfoil with diameter D across the stream (with one degree of freedom). Airfoil constrain is assumed to be linear viscoelastic and its motion (4) is described by the following ordinary differential equation:

$$m\ddot{y}_* + b\dot{y}_* + cy_* = F_y. \tag{12}$$

Here m is the airfoil mass, b is a small damping factor, c is the constraint rigidity, F_y is lift force, y_* is the deviation from the equilibrium. The natural frequency of the system $\omega \approx \sqrt{c/m}$ can be set by varying of the coefficient c.

The deviation from the equilibrium on the n-th step of computation is $y_*^n = Y_C^n - Y_C^0$. Here Y_C^0 is the ordinate of the airfoil center at the initial time and Y_C^n is the ordinate of the airfoil center at the n-th step of computation. Difference analogue of the equation (12) can be written down in the following form:

$$m \cdot \frac{Y_C^{n+1} - 2Y_C^n + Y_C^{n-1}}{(\Delta t)^2} + b \cdot \frac{Y_C^{n+1} - Y_C^{n-1}}{2\Delta t} + c \cdot (Y_C^n - Y_C^0) = F_y|^n. \tag{13}$$

Position of the airfoil center at the next time step can be easily obtained from this equation on every computational step after computing the lift force acting on the airfoil. It allows to reconstruct the level-set function and all matrices required for the computation and to compute the immersed boundary velocity $\mathbf{v}^{ib}$ for recalculation the source terms.

Number of computations have been performed on non-uniform grid 272×292 with time discretization step $\Delta t = 0.0001$ and the following dimensionless parameters:

$$V_\infty = 3.0, \quad \rho = 1.0, \quad \nu = 0.003, \quad D = 1.0, \quad m = 39.75, \quad b = 0.731.$$

These parameters correspond to the Reynolds number Re = 1000. The dimensionless natural frequency of the system is in the following range:

$$\mathrm{St}_\omega = \frac{\omega}{2\pi} \cdot \frac{D}{V_\infty} = 0.150 \ldots 0.280.$$

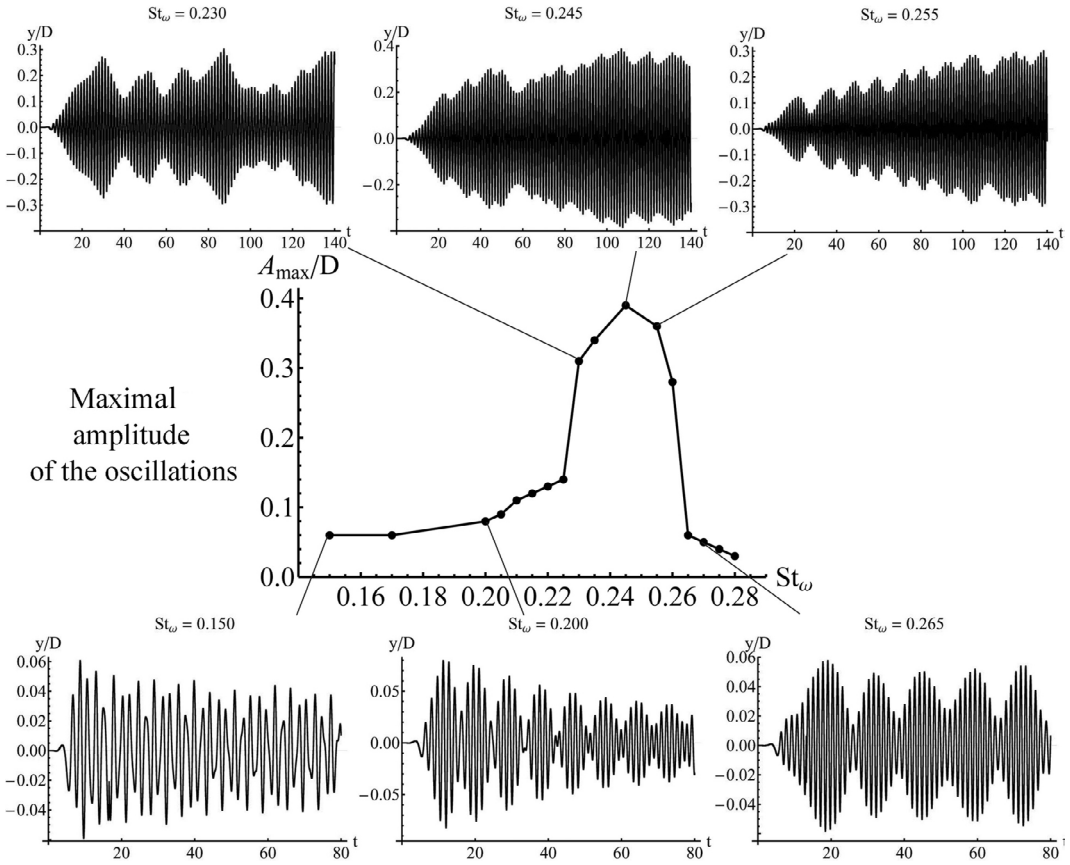

Figure 3: Maximal amplitude of the circular airfoil oscillations at Re = 1000

Computational results are in good agreement with the previous studies [9]. Maximal amplitude (fig. 3) is about $0.4D$ and it occures when the natural frequency of the system St_ω is close to the Strouhal number, calculated for a fixed airfoil $\mathrm{St} \approx 0.24$ [2, 10, 11].

Qualitative differences in airfoil dynamics at Strouhal numbers in investigated region are shown on fig. 3. Slight airfoil vibration is observed when the natural frequency of the system is significantly less than the frequency of vortex shedding. Damped beats appear with increasing natural frequency as you get closer to the Strouhal number. Amplitude of the oscillations increases sharply near the frequency of vortex shedding. Beats disappear and amplitude continues to increase with time. Amplitude of the oscillations decreases sharply and beats are observed again with a further increase of the St_ω.

4.2 Circular airfoil buffeting

To simulate buffeting phenomenon we considered the motion of two equal circular airfoils with diameter $D = 1.0$ across the stream at $V_\infty = 1.0$ (with two degrees of freedom). The distance between airfoils centers is equal to $L = 5.5$ on the horizontal and $T = 0.7$ on the vertical at the initial time. Airfoils constrains are assumed to be linear viscoelastic (fig. 4) and their motion (4) is described by the following equations:

$$m\ddot{x}_{*,i} + b\dot{x}_{*,i} + cx_{*,i} = F_{x,i}, \quad m\ddot{y}_{*,i} + b\dot{y}_{*,i} + cy_{*,i} = F_{y,i}, \quad i = \overline{1,N}. \tag{14}$$

Here $m = 4.7273$ is the airfoil mass, $b = 4\pi m\xi \mathrm{St}_\omega$ is the damping factor, $\xi = 3.3 \cdot 10^{-4}$, $c = m(2\pi \mathrm{St}_\omega)^2$ is the constraints rigidity; $N = 2$ is a number of airfoils, F_x and F_y are drag and lift forces, x_* and y_* are the deviations from the equilibrium on Ox and Oy.

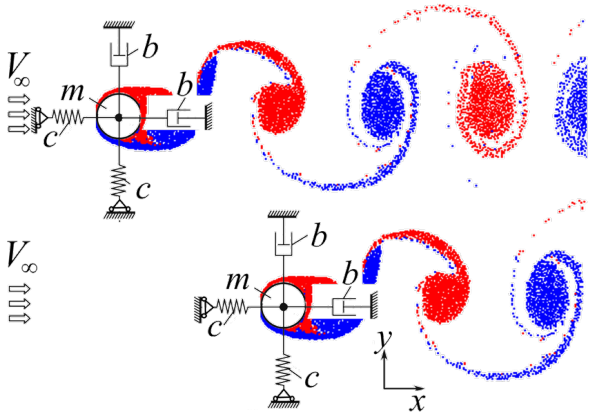

Figure 4: Circular airfoils with Kelvin — Voigt viscoelastic constraints and vortex wake behind them

The deviations from the equilibrium on the n-th step of computation are $x^n_{*,i} = X^n_{C,i} - X^0_{C,i}$, $y^n_{*,i} = Y^n_{C,i} - Y^0_{C,i}$. Here $(X^0_{C,i},\ Y^0_{C,i})$ are coordinates of the airfoil center at the initial time and $(X^n_{C,i},\ Y^n_{C,i})$ are coordinates of the airfoil center at the n-th step of computation. Difference analogues of equations (14) can be written down in the following form:

$$m \cdot \frac{X^{n+1}_{C,i} - 2X^n_{C,i} + X^{n-1}_{C,i}}{(\Delta t)^2} + b \cdot \frac{X^{n+1}_{C,i} - X^{n-1}_{C,i}}{2\Delta t} + c \cdot (X^n_{C,i} - X^0_{C,i}) = F_{xa,i}|^n, \tag{15}$$

$$m \cdot \frac{Y^{n+1}_{C,i} - 2Y^n_{C,i} + Y^{n-1}_{C,i}}{(\Delta t)^2} + b \cdot \frac{Y^{n+1}_{C,i} - Y^{n-1}_{C,i}}{2\Delta t} + c \cdot (Y^n_{C,i} - Y^0_{C,i}) = F_{ya,i}|^n. \tag{16}$$

Computations have been performed on non-uniform grid 666×344 at $\mathrm{Re} = 100$ and $\mathrm{Re} = 1000$. The dimensionless natural frequency of the system was in the range $\mathrm{St}_\omega/\mathrm{St} = 0.50 \ldots 2.00$. Here St is the Strouhal number, calculated for a fixed airfoil at the corresponding Reynolds number. Time discretization step was equal to $\Delta t = 10^{-4}$ ($\Delta t = 5 \cdot 10^{-5}$ at $\mathrm{Re} = 1000$) at $\mathrm{St}_\omega/\mathrm{St} = 0.85 \ldots 1.15$ and $\Delta t = 5 \cdot 10^{-4}$ ($\Delta t = 10^{-4}$ at

$\mathrm{Re} = 1000$) at $\mathrm{St}_\omega/\mathrm{St} = \{0.50, 0.70, 1.40 \ldots 2.00\}$. The uniform mesh block with spatial discretization step $h = D/64$ was used in the proximity of the airfoil.

Since the distance between the airfoils centers along Ox axis is large enough ($> 5D$), upstream airfoil (K_1) behaves like a single airfoil and downstream airfoil (K_2) performs forced oscillations due to periodic vortex-shedding flow past airfoil K_1. Thus, buffeting of airfoil K_2 is observed. Maximal amplitude of the airfoil K_2 oscillations significantly exceeds amplitude of the airfoil K_1 oscillations at $\mathrm{Re} = 100$ (fig. 5). Maximal amplitude of the airfoil K_1 oscillations appear at $\mathrm{St}_\omega \approx \mathrm{St}$ ($\mathrm{St} \approx 0.162$ at $\mathrm{Re} = 100$) as in [12]. This corresponds to the single airfoil behavior in the flow. Maximal amplitude of the airfoil K_2 oscillations along Oy axis appears at $\mathrm{St}_\omega \approx 0.85\mathrm{St}$. Amplitude of airfoil K_2 oscillations along Oy axis is less than amplitude of airfoil K_1 oscillations (fig. 6) at $\mathrm{Re} = 1000$ as in [13]. In this case maximal amplitude of the circular airfoils oscillations appears at $\mathrm{St}_\omega \approx \mathrm{St}$ both along Oy axis and Ox axis.

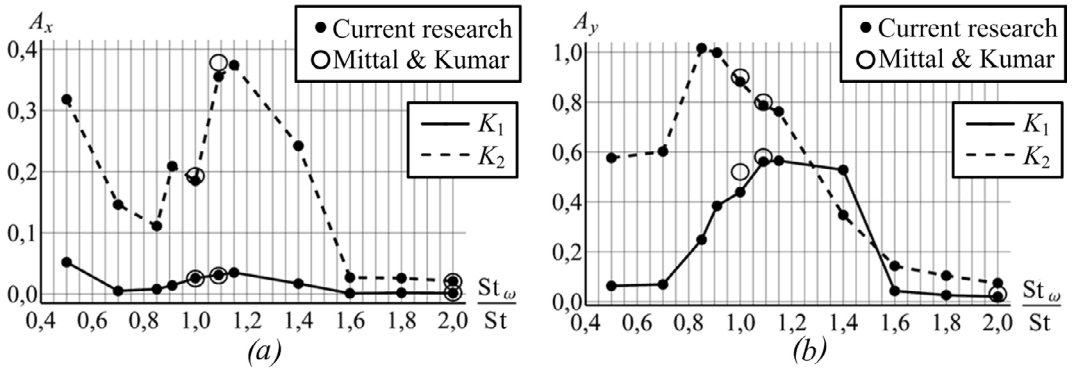

Figure 5: Maximal amplitude of the circular airfoils oscillations at $\mathrm{Re} = 100$: *(a)* along Ox axis; *(b)* along Oy axis

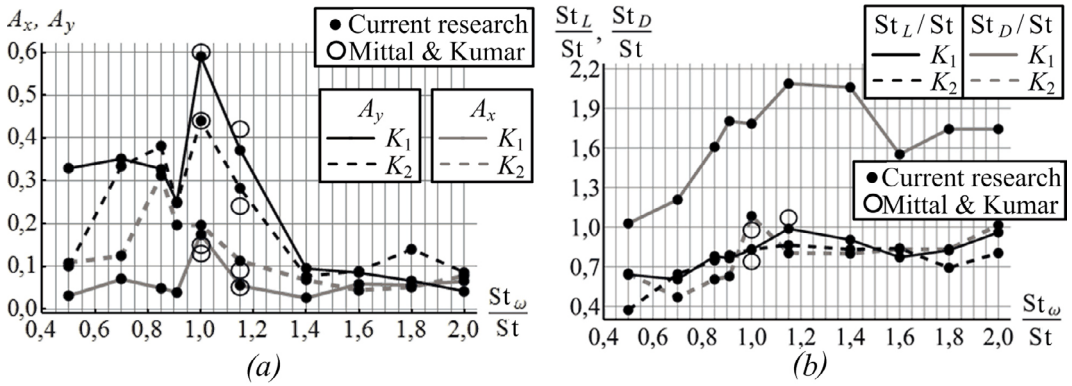

Figure 6: Characteristics of the circular airfoils oscillations at $\mathrm{Re} = 1000$: *(a)* maximal amplitude of the circular airfoils oscillations; *(b)* frequences of lift and drag forces oscillations

4.3 Tube-bundle flow-induced vibrations

We considered the motion of circular airfoils with diameter $D = 1.0$ across the stream at $V_\infty = 1.0$ (with two degree of freedom). Airfoils constrains are assumed to be linear viscoelastic (fig. 4) and their motion (4) is described by the ordinary differential equations (14). Tubes can be destroyed at $\mathrm{St}_\omega \approx \mathrm{St}$ with damping, which corresponds to the damping coefficient $b < 0.1$ [14]. Therefore, simulations were performed at $m = 40$ and $\xi = 3.3 \cdot 10^{-3}$ in this research. These values correspond to the damping coefficient $b = 4\pi m \xi \mathrm{St}_\omega > 0.14$ at $\mathrm{St}_\omega > 0.09$.

Flow pattern depends on the tubes arrangement and tube locations in the bundle [14]. For this reason, we considered flow around six columns of tubes in staggered arrangement and flow around five columns of tubes in in-line arrangements (fig. 7).

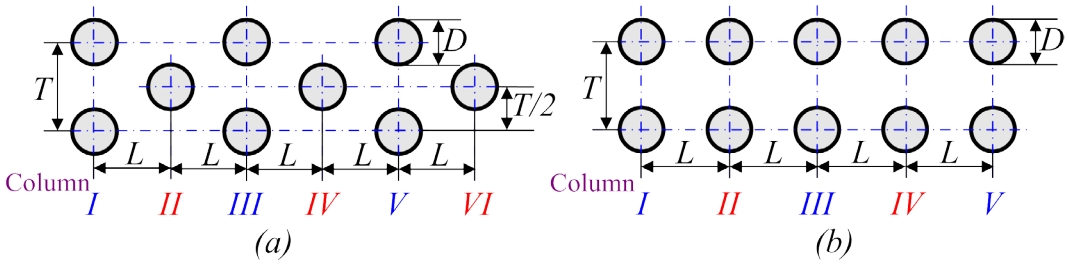

Figure 7: Considered tube arrangements: *(a)* staggered tube arrangement; *(b)* in-line tube arrangement

The distances between airfoils centers are equal to L on the horizontal and T on the vertical at the initial time. When the simulation was performed at $T/D > 4$, vortex streets between the rows do not affect each other, as in [14]. When $L/D > 4$, tubes in the bundle behave as single airfoils.

So, tube-bundle behaves as a single system at lower values of L, T. As an example, here we present computational results at $T/D = 2.0$, $L = T$ in case of in-line tube arrangement and $L = T\sqrt{3}/2$ in case of staggered tube arrangement. Thus, in the first case airfoils in adjacent columns are in the corners of a square, and in the second case they are located at the vertices of an equilateral triangle.

Number of computations have been performed at $\mathrm{Re} = 1000$ on non-uniform grid 846×424 in case of staggered tube arrangement and on non-uniform grid 816×424 in case of in-line tube arrangement. The uniform mesh block with space discretization step $h = D/64$ was used in the vicinity of the airfoil. Time discretization step was equal to $\Delta t = 5 \cdot 10^{-5}$. Computations were performed on a server based on the Intel C610 platform using the Intel Xeon E5-1620 V3 4-core processor (3.5 GHz) with HyperThreading support (8 logical cores). The server is equipped with 16 GB of ECC DDR4-2133 RAM and two hard drives (2 TB), united in a RAID1 disk volume. This server is running Windows Server 2012 R2 operating system. To simulate 50 dimensionless time units it is required about 137 hours.

The natural frequency of the system was in range $\mathrm{St}_\omega/\mathrm{St} = 0.50 \ldots 2.00$. Here St is the Strouhal number, calculated for a fixed tube-bundle at the corresponding Reynolds number. Our simulations showed that $\mathrm{St} \approx 0.205$ in case of in-line tube arrangement. This is in agreement with the fact that for this arrangement in the experiments [14] $\mathrm{St} = \mathrm{St}(T/D) = 0.2 + \exp[-1.2(T/D)^{1.8}]$, i.e. $\mathrm{St}(2.0) \approx 0.215$. In case of staggered arrangement two different frequencies are observed for tubes from even and odd columns (fig. 7) as in [14]. Upper frequency is observed in the tubes from odd columns. This frequency is considered as the vortex shedding frequency. So, we obtain that $\mathrm{St} \approx 0.280$ in case of staggered tube arrangement. This is in agreement with the fact that in the experiments [14] the maximum amplitude of oscillation occurs at a frequency equal to $(0.4 + 2\exp[-0.44(T/D)^{1.8}])/3$, i.e $\mathrm{St} \approx 0.277$ at $T/D = 2.0$. Lower frequency is observed in the tubes from even columns and it is equal St/2. It corresponds to frequency of vortex street interaction.

Computational results (fig. 8) are in qualitative agreement with the experimental data [14]. Tubes from first column behave like a single airfoils. In case of staggered tubes arrangement amplitude of the tubes oscillations along Oy axis significantly decreases with increasing column number.

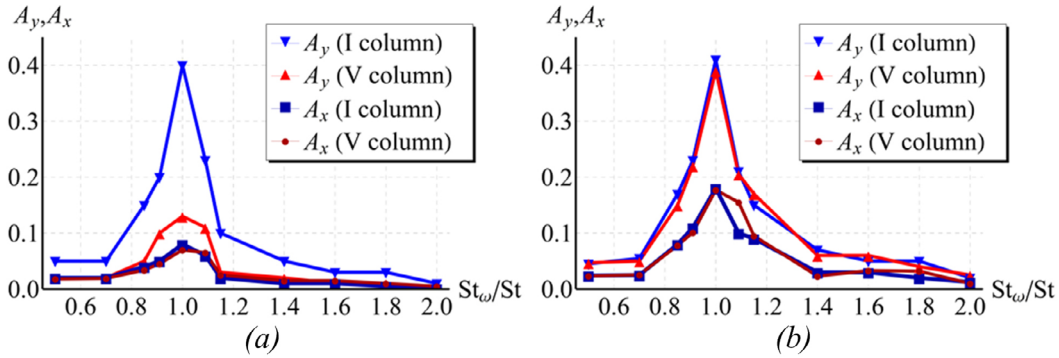

Figure 8: Maximal amplitude of the tubes oscillations at $\mathrm{Re} = 1000$: *(a)* staggered tube arrangement; *(b)* in-line tube arrangement

5 CONCLUSIONS

- A software package is developed for the numerical simulation of the airfoils motion in the viscous incompressible flow by using the LS-STAG method.
- Simulation of a circular airfoil wind resonance and buffeting phenomenons, tube-bundle flow-induced vibrations are considered. The LS-STAG method allows to simulate these phenomenons on a very coarse mesh.
- Computational results are in good qualitative agreement with the experimental data.

6 ACKNOWLEGEMENTS

The work was partially supported by Russian Federation President Grant for young scientists [proj. MK-7431.2016.8].

REFERENCES

[1] Mittal, R. and Iaccarino, G. Immersed boundary methods. *Annu. Rev. Fluid Mech.* (2005) **37**:239–261.

[2] Cheny, Y. and Botella, O. The LS-STAG method: A new immersed boundary/level-set method for the computation of incompressible viscous flows in complex moving geometries with good conservation properties. *J.Comput.Phys.* (2010) **229**:1043–1076.

[3] Osher, S. and Fedkiw, R.P. *Level set methods and dynamic implicit surfaces.* Springer, (2003).

[4] Van der Vorst, H.A. Bi-CGSTAB: a fast and smoothly converging variant of Bi-CG for solution of non-symmetric linear systems. *SIAM J. Sci. Stat. Comp.* (1992). **2**:631–644.

[5] Wesseling, P. *An introduction to multigrid methods.* John Willey & Sons Ltd., (1991).

[6] Van Kan, J., Vuik, C. and Wesseling, P. Fast pressure calculation for 2D and 3D time dependent incompressible flow. *Numer. Lin. Alg. Appl.* (2000) **7**:429–447.

[7] Marchevsky, I.K. and Puzikova, V.V. OpenFOAM iterative methods efficiency analysis for linear systems solving. *Proceedings of the Institute for System Programming of RAS.* (2013) **24**:71–86. [in Russian]

[8] Marchevskii, I.K. and Puzikova, V. V. Numerical simulation of the flow around two fixed circular airfoils positioned in tandem using the LS-STAG method. *J. Mach. Manuf. Reliab.* (2016) **45**:130–136.

[9] Klamo, J.T., Leonard, A. and Roshko, A. On the maximum amplitude for a freely vibrating cylinder in cross flow. *J. of Fluids and Struct.* (2005) **21**:429–434.

[10] He J.W., Glovinski, R., Metcalfe, R., Nordlander, A. and Triaux, J.P. Active control and drag optimization for flow past a circular cylinder. Part I: Oscillatory cylinder rotation. *J. Comput. Phys.* (2000) **163**:87–117.

[11] Henderson, R.D. Nonlinear dynamics and pattern formation in turbulent wake transition. *J. Fluid Mech.* (1997) **352**:65–112.

[12] Mittal, S. and Kumar, V. Flow-induced oscillations of two cylinders in tandem and staggered arrangements. *J. Fluids Struct.* (2001) **15**:717–736.

[13] Mittal S. and Kumar, V. Vortex induced vibrations of a pair of cylinders at Reynolds number 1000. *Int. J. Comput. Fluid Dyn.* (2004) **18**:601–614.

[14] Zukauskas, A., Ulinskas, R. and Katinas, V. *Gidrodinamika i vibratsii obtekayemykh puchkov trub (Fluid Dynamics and Flow-Induced Vibrations of Tube Banks).* Vil'nyus, (1984).